International Journal of Emerging Research in Engineering, Science, and Management
Vol. 5 | Issue 1 | pp. 32-41 | Jan-Mar 2026.
www.ijeresm.com | eISSN – 2583-4894
Received: 22 Nov 2025 | Revised: 16 Feb 2026 | Accepted: 23 Feb 2026 | Published: 01 Mar 2026

Substrate-Dependent Performance Evaluation of a DGS-Based Multiband Hexagonal Microstrip Patch Antenna for 5G FR2 Applications

[1]Yuvaraj K, [2]Sanam Narayana Reddy

[1]Research Scholar, Department of Electronics and Communication Engineering, Sri Venkateswara University College of Engineering, Tirupati, India. yuvaraj.kunati@gmail.com, ORCID ID: 0009-0003-6622-199X.
[2]Professor, Department of Electronics and Communication Engineering, Sri Venkateswara University College of Engineering, Tirupati, India. snreddysvu@yahoo.com, ORCID ID: 0000-0002-3638-1357.

Abstract: This paper presents a substrate-dependent performance evaluation of a defected ground structure (DGS)-integrated multiband hexagonal microstrip patch antenna operating in the 22–28 GHz millimetre-wave band for 5G FR2 applications. To examine the influence of dielectric properties on electromagnetic behaviour, the same antenna geometry is implemented on three commonly used substrates—Duroid (relative permittivity $\varepsilon_r \approx 2.2$, loss tangent $\tan\delta \approx 0.0009$), Rogers ($\varepsilon_r \approx 2.94$, $\tan\delta \approx 0.0012$), and FR4 ($\varepsilon_r \approx 4.4$, $\tan\delta \approx 0.02$). A controlled substrate-based comparison is conducted with respect to the reflection coefficient, impedance bandwidth, gain, and radiation efficiency. The results indicate that substrate characteristics significantly affect resonance depth, impedance stability, and radiation performance at millimetre-wave frequencies. The Duroid-based configuration achieves S_{11} below −32 dB, peak gain of 8–8.5 dBi, and high radiation efficiency due to reduced dielectric loss. The Rogers substrate exhibits stable multiband behaviour with moderate gain, whereas the FR4-based design shows reduced resonance depth and lower gain due to increased dielectric dissipation. By maintaining identical geometry across all substrates, the study isolates the direct impact of dielectric constant and loss tangent on modal excitation and efficiency degradation in the 22–28 GHz band. The presented analysis supports informed substrate selection for compact multiband mmWave antenna designs in next-generation wireless systems.

Keywords: Millimetre-Wave Antenna, Hexagonal Microstrip Antenna, Defected Ground Structure (DGS), Multiband Operation, Substrate-Dependent Analysis, 5G NR FR2.

1 Introduction

The utilisation of millimetre-wave (mmWave) frequency bands in 5G Frequency Range-2 (FR2) and emerging 6G systems has significantly increased the demand for compact, high-gain, and multiband antennas capable of supporting high data rates. Microstrip patch antennas remain widely adopted due to their low profile, light weight, ease of fabrication, and compatibility with planar RF circuitry [1]. However, antenna performance at mmWave frequencies is strongly influenced by the dielectric properties of the material. The substrate dielectric constant and loss tangent play a critical role in determining impedance behaviour, radiation efficiency, and gain. Lower dielectric constants generally improve radiation efficiency and reduce surface-wave losses, whereas higher-permittivity substrates tend to confine fields and may reduce overall radiation performance [2][3]. At mmWave frequencies, dielectric losses become more pronounced, making substrate selection a key design consideration.

Several recent works have proposed wideband and multiband mmWave antennas for 5G and beyond [4]-[6], employing techniques such as slot loading, reconfigurable structures, multiple resonance modes, and parasitic elements to enhance bandwidth and support multiband operation [7][8]. In addition, MIMO and array configurations have been investigated to improve channel capacity and isolation in compact wireless platforms [9]–[11]. Low-loss substrates such as Rogers and Duroid have been widely reported to improve impedance bandwidth and radiation efficiency at high frequencies [12], while FR4, despite its low cost and mechanical robustness, exhibits increased dielectric loss at mmWave frequencies [4]. Although substantial research has focused on geometry optimisation and DGS-based bandwidth enhancement, systematic investigations that isolate substrate-dependent electromagnetic behaviour while maintaining identical antenna geometry remain limited in the mmWave regime.

In many reported studies, geometry and material parameters are varied simultaneously, making it difficult to quantify the direct impact of dielectric constant and loss tangent on resonance formation and efficiency degradation [13]. In this work, a controlled substrate-dependent evaluation is performed by implementing the same DGS-integrated hexagonal patch geometry on Duroid, Rogers, and FR4 substrates. By eliminating geometric variability, the study directly correlates dielectric properties with resonance sharpness, multiband stability, impedance behaviour, and radiation efficiency in the 22–28 GHz band.

International Journal of Emerging Research in Engineering, Science, and Management
Vol. 5 | Issue 1 | pp. 32-41 | Jan-Mar 2026.
www.ijeresm.com | eISSN – 2583-4894
Received: 22 Nov 2025 | Revised: 16 Feb 2026 | Accepted: 23 Feb 2026 | Published: 01 Mar 2026

The main contributions of this work are summarised as follows:

1. A substrate-controlled comparative analysis of Duroid, Rogers, and FR4 using identical antenna geometry in the 22–28 GHz band.
2. Quantitative evaluation of impedance matching, bandwidth, gain, and efficiency for each substrate configuration.
3. Assessment of dielectric-loss-induced performance degradation at mmWave frequencies under fixed structural conditions.

This approach provides a structured framework for substrate selection in compact multiband mmWave antenna design.

2 METHODOLOGY

The proposed multiband hexagonal microstrip patch antenna is designed to operate within the 22–28 GHz mmWave band. The design methodology includes substrate selection, the geometrical configuration of the hexagonal patch, the feeding mechanism, and the integration of a defected ground structure (DGS) to enhance impedance bandwidth and modal stability. Electromagnetic simulations were performed using HFSS to evaluate impedance and radiation characteristics. The simulated model of the antenna structure is shown in Fig. 1.

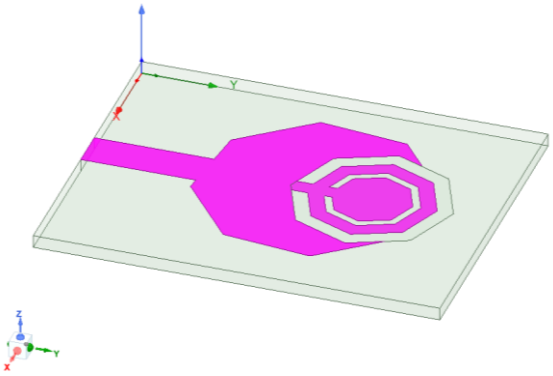

Fig. 1. Simulation model of Multiband Hexagonal Patch Antenna

2.1. Substrate and Material Selection

The antenna geometry is implemented on three widely used substrates: Duroid ($\varepsilon_r \approx 2.2$, $\tan\delta \approx 0.0009$), Rogers ($\varepsilon_r \approx 2.94$, $\tan\delta \approx 0.0012$), and FR4 ($\varepsilon_r \approx 4.4$, $\tan\delta \approx 0.02$). A uniform substrate thickness of 1.6 mm is maintained for all configurations to ensure controlled comparison. The design variables are given in Table 1.

Table 1. Design Variables Used in the Simulation

Name	Value (mm)
Ground Width (W_g)	40
Ground Length (L_g)	50
Substrate Length (L_s)	50
Substrate Width (W_s)	40
Substrate Thickness (T)	1.6
Feed Width (W_f)	5
Feed Length (L_f)	27
Patch Width (W_p)	35
Patch Length (L_p)	25

To maintain consistency in comparative evaluation, manufacturer-specified dielectric properties were used. FR4 exhibits frequency-dispersive behaviour at mmWave frequencies; however, constant permittivity and loss tangent values were used to enable uniform analysis across substrates. The selected thickness of 1.6 mm reduces the effective quality factor and enhances fringing fields, contributing to bandwidth improvement. Although thicker substrates may introduce surface-wave excitation at mmWave frequencies, the integrated DGS perturbs the return-current path and suppresses propagation of higher-order modes. Simulated radiation patterns confirm that back-lobe enhancement remains limited within the operating band.

International Journal of Emerging Research in Engineering, Science, and Management
Vol. 5 | Issue 1 | pp. 32-41 | Jan-Mar 2026.
www.ijeresm.com | eISSN – 2583-4894
Received: 22 Nov 2025 | Revised: 16 Feb 2026 | Accepted: 23 Feb 2026 | Published: 01 Mar 2026

2.2. Hexagonal Patch Geometry

A hexagonal patch geometry is selected for its efficient area utilisation and its ability to support multiple resonant modes [14]. Based on the cavity-model approximation, the fundamental resonant frequency is determined using standard microstrip-antenna relations. The resonance frequency is calculated using Eq. (1).

$$f_r = \frac{C\, X_{mn}}{2\pi a_{eq}\sqrt{\varepsilon_{eff}}} \tag{1}$$

where:

- f_r is the desired resonant frequency,
- C is the velocity of light,
- a_{eq} is the effective radius of the hexagon ring = $\sqrt{\frac{2\,A}{3\sqrt{3}}}$
- A is the physical area of the hexagon
- ε_{eff} is the effective dielectric constant.

The effective dielectric constant is calculated using Eq. (2).

$$\varepsilon_{eff} = \frac{\varepsilon_r+1}{2} + \frac{\varepsilon_r-1}{2}\left(1 + 12\frac{h}{W_p}\right)^{-0.5} \tag{2}$$

where h is the substrate height, and Wp is the patch width. In this design: h=1.6 mm, ε_r=2.2, and Wp=35mm. The patch radius is calculated using Eq. (3).

$$r = \frac{F}{[1+\frac{2h}{\varepsilon_r \pi F}\{\ln\left(\frac{\pi F}{2h}\right)+1.7726\}]^{1/2}} \tag{3}$$

where F is given in Eq. (4).

$$F = \frac{8.791\times10^8}{f_r\sqrt{\varepsilon_r}} \tag{4}$$

The effective radius of the patch is given by Eq. (5).

$$r_e = r\left[1 + \frac{2h}{\varepsilon_r \pi F}\left\{\ln\left(\frac{\pi F}{2h}\right) + 1.7726\right\}\right]^{1/2} \tag{5}$$

2.3. Feeding Technique

A microstrip line feed is employed due to its planar configuration and ease of impedance matching [15]. The feed dimensions (W_f = 5 mm, L_f = 27 mm) are optimised to achieve an input impedance of approximately 50 Ω. The characteristic impedance is given by Eq. (6).

$$Z_0 = \frac{60}{\sqrt{\varepsilon_{eff}}}\ln\left[\frac{8h}{W_f} + \frac{W_f}{4h}\right] \tag{6}$$

where,

Z_0 is the characteristic impedance of the feedline.

The approximate impedance bandwidth is given by Eq. (7).

$$\text{Bandwidth, BW} \approx \frac{1.5\,h}{\lambda_0\sqrt{\varepsilon_r}} \tag{7}$$

2.4. Ground Plane and DGS Integration

A circular defected ground structure (DGS) is introduced beneath the feed region to modify the current distribution and introduce additional reactive loading [16]. The DGS generates an equivalent parallel LC resonance, reducing the effective quality factor and enhancing impedance bandwidth. The DGS slot is patterned circularly to resonate at multiple frequencies. The presence of DGS alters the current distribution on the ground plane, resulting in a slow-wave effect that improves isolation and bandwidth. The equivalent inductance L_g and capacitance C_g introduced by the DGS slot can be modelled by Eq. (8).

International Journal of Emerging Research in Engineering, Science, and Management
Vol. 5 | Issue 1 | pp. 32-41 | Jan-Mar 2026.
www.ijeresm.com | eISSN – 2583-4894
Received: 22 Nov 2025 | Revised: 16 Feb 2026 | Accepted: 23 Feb 2026 | Published: 01 Mar 2026

$$f_{DGS} = \frac{1}{2\pi\sqrt{L_g C_g}} \quad (8)$$

where f_{DGS} is the resonance frequency of DGS
L_g is Effective inductance
C_g is the Effective capacitance

By considering the curve fitting method from the simulated responses, the extracted equivalent parameters from the curve fitting of the simulated S_{11} response are:

$$L \approx 0.42 \text{ nH}$$
$$C \approx 0.18 \text{ pF}$$

Fig. 2 shows an equivalent circuit model for the DGS-Integrated hexagonal patch antenna. The equivalent LC model closely reproduces the simulated resonance behaviour, validating the reactive perturbation introduced by the DGS. The S_{11} curve was used to establish the resonant frequency, and the −3 dB bandwidth was used to calculate the quality factor. L = 0.42 nH and C ≈ 0.18 pF were obtained by solving the resonance and Q-factor equations simultaneously. The tight match between the simulated frequency response and the reconstructed LC resonance validates the equivalent circuit model. By introducing a slow-wave effect, these reactive components improve impedance matching and lower the effective propagation constant. The defective ground structure functions as an engineered reactive perturbation that modifies the effective inductive–capacitive behaviour of the ground plane, thereby reducing the quality factor and enhancing impedance bandwidth without increasing structural complexity.

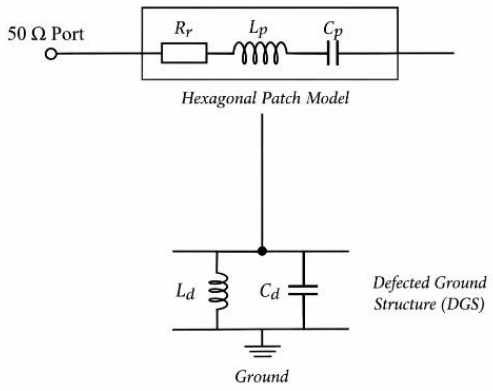

Fig. 2. Equivalent Circuit Model for DGS- Integrated hexagonal patch antenna

2.5. Bandwidth Optimisation

The fractional bandwidth BW% of the antenna is calculated using Eq. (9).

$$BW\% = \frac{f_{high} - f_{low}}{f_{center}} \times 100 \quad (9)$$

where f_{low} and f_{high} are the lower and upper -10 dB return loss points, and f_{center} is the centre frequency. For the optimised Duroid-based configuration, the measured −10 dB cutoff frequencies were 26.25 GHz and 27.35 GHz, corresponding to a centre frequency of 26.8 GHz. Substituting these values into Eq. (9) results in a fractional bandwidth of approximately 4.1%. This confirms that the proposed structure achieves stable impedance performance within the intended millimetre-wave operating band. The observed bandwidth improvement is primarily attributed to the incorporation of the defected ground structure (DGS). The presence of the DGS perturbs the surface current distribution beneath the radiating element and introduces additional reactive loading in the ground plane. This effectively lowers the antenna quality factor and moderates the impedance slope around resonance, thereby widening the −10 dB operating region. A similar calculation for the lower band yields a fractional bandwidth of approximately 3.67%.

In contrast to conventional bandwidth enhancement techniques—such as stacked configurations, parasitic patches, or multilayer substrates—the proposed approach employs a single-layer planar DGS modification. This method preserves structural simplicity while maintaining electromagnetic effectiveness. The key practical benefits include:

- Compatibility with standard PCB fabrication processes
- Retention of compact size and low-profile geometry
- Bandwidth enhancement without noticeable gain degradation

International Journal of Emerging Research in Engineering, Science, and Management
Vol. 5 | Issue 1 | pp. 32-41 | Jan-Mar 2026.
www.ijeresm.com | eISSN – 2583-4894
Received: 22 Nov 2025 | Revised: 16 Feb 2026 | Accepted: 23 Feb 2026 | Published: 01 Mar 2026

As a result, the antenna achieves improved fractional bandwidth while preserving stable radiation characteristics and structural compactness. These attributes make the design well-suited for practical millimetre-wave wireless applications, where performance reliability and ease of fabrication are equally important.

2.6. Experimental Validation

The antenna prototype was fabricated using standard PCB manufacturing techniques based on the optimised simulated dimensions, as shown in Fig. 3. The reflection coefficient (S_{11}) was measured using a calibrated vector network analyser over the 22–28 GHz frequency range. Prior to measurement, standard calibration procedures were performed to minimise systematic errors. Radiation characteristics were evaluated under controlled laboratory conditions using a standard antenna measurement setup. The antenna under test was positioned appropriately to ensure far-field conditions, and measured responses were compared with simulated results to validate performance trends. Minor discrepancies between simulated and measured responses are attributed to fabrication tolerances, connector losses, and material property variations at millimetre-wave frequencies.

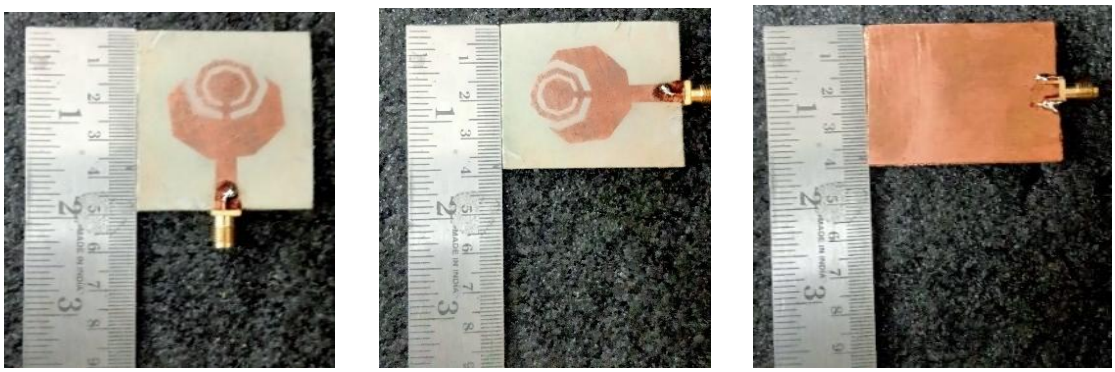

Fig. 3. Fabrication Model of Hexagonal Patch Antenna

3 Results and Discussion

3.1. Return Loss Behaviour

The simulated reflection coefficient (S_{11}) characteristics of the proposed hexagonal patch antenna on Duroid, Rogers, and FR4 substrates are illustrated in Fig. 4. For the Duroid-based configuration, two dominant resonant frequencies are observed at 23.2 GHz and 26.8 GHz, with reflection coefficients reaching approximately −32 dB and −35 dB, respectively. These deep and sharp minima indicate good impedance matching and strong energy confinement. However, the number of significant resonances is limited to these two well-defined modes, suggesting stable dual-band behaviour with high resonance quality. In contrast, the FR4 substrate exhibits resonant dips at approximately 22.5 GHz and 26.2 GHz, with S_{11} values ranging from −12 dB to −15 dB. The shallower depth and slight frequency shifts indicate dielectric loss effects and reduced resonance sharpness. At millimetre-wave frequencies, FR4's higher loss tangent contributes to energy dissipation in the substrate, broadening resonances and weakening impedance stability. As a result, although dual-band behaviour is present, the resonance quality is comparatively lower.

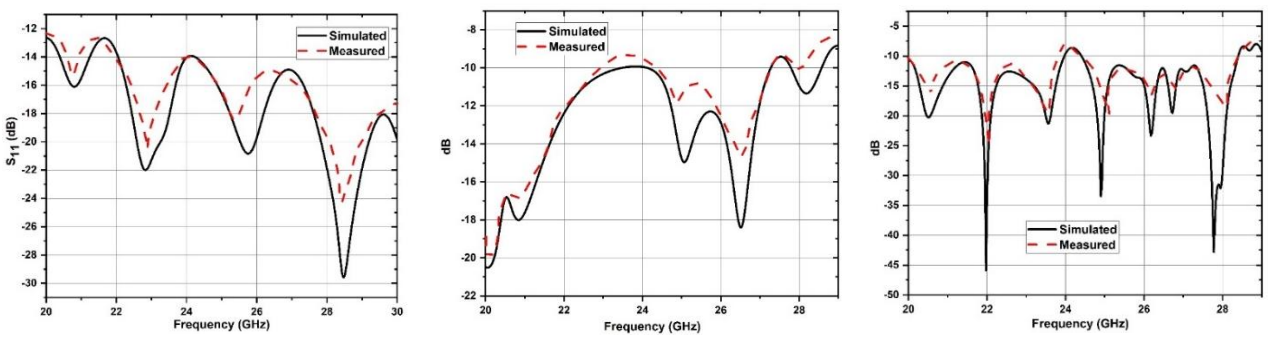

Fig. 4. S_{11} Plots of hexagonal ring for Duroid, FR4 & Rogers

International Journal of Emerging Research in Engineering, Science, and Management
Vol. 5 | Issue 1 | pp. 32-41 | Jan-Mar 2026.
www.ijeresm.com | eISSN – 2583-4894
Received: 22 Nov 2025 | Revised: 16 Feb 2026 | Accepted: 23 Feb 2026 | Published: 01 Mar 2026

The Rogers substrate shows multiple distinct S_{11} minima at approximately 23.0 GHz, 25.4 GHz, and 26.5 GHz, all below the −10 dB threshold, with reflection coefficients ranging from −24 dB to −28 dB. The presence of three identifiable resonant dips confirms the excitation of additional modes, indicating stronger multiband characteristics than those of Duroid and FR4. The moderate dielectric constant and relatively low loss tangent of Rogers allow sufficient energy storage while enabling excitation of multiple resonant current distributions. From an electromagnetic perspective, these multiple resonances arise from different surface-current modes supported by the hexagonal patch and from its interaction with the defective ground structure. Substrate properties influence how effectively these modes are sustained. Low-loss substrates such as Duroid support sharper and deeper resonances, whereas moderate-permittivity materials like Rogers facilitate excitation of multiple radiating modes without excessive damping. The frequency-specific S_{11} analysis confirms that:

- **Duroid:** Dual-band operation at 23.2 GHz and 26.8 GHz with strong impedance matching.
- **FR4:** Dual-band behaviour at 22.5 GHz and 26.2 GHz, with reduced resonance depth due to dielectric loss.
- **Rogers:** Multiband response at 23.0 GHz, 25.4 GHz, and 26.5 GHz, supporting multiple usable resonances.

These results indicate that substrate selection influences the sharpness of resonances, modal excitation, and multiband stability in millimetre-wave patch antennas. The resonant frequencies and bandwidths are given in Table 2.

Table 2. Resonant Frequency and Bandwidth Summary

Substrate	Band	f_{low} (GHz)	f_{high} (GHz)	centre (GHz)	Bandwidth (GHz)	Fractional BW (%)
Duroid	Band 1	22.75	23.60	23.18	0.85	3.67
	Band 2	26.25	27.35	26.80	1.10	4.10
Rogers	Band 1	22.65	23.35	23.00	0.70	3.04
	Band 2	25.00	25.80	25.40	0.80	3.15
	Band 3	26.10	27.05	26.58	0.95	3.57
FR4	Band 1	22.20	22.75	22.48	0.55	2.44
	Band 2	25.85	26.55	26.20	0.70	2.67

The results indicate that multiband behaviour is substrate-dependent rather than purely geometry-driven, with Rogers exhibiting three stable resonances while Duroid and FR4 primarily support dual-band operation.

3.2. VSWR Comparison for Multiband Evidence

The corresponding Voltage Standing Wave Ratio (VSWR) characteristics for the three substrate configurations are shown in Fig. 5. VSWR remains below 2 primarily around the dominant resonant frequencies for the Duroid configuration. Outside these regions, the VSWR increases rapidly. This indicates that Duroid provides efficient impedance matching within limited frequency bands, supporting stable dual-band operation rather than extended multiband behaviour. For the FR4 substrate, the VSWR response fluctuates significantly across the operating range. Several frequency regions approach or exceed the acceptable limit (VSWR > 2), and the band edges are less well defined. This behaviour suggests reduced impedance stability, which may be attributed to higher dielectric loss and dispersion effects at millimetre-wave frequencies. The Rogers substrate exhibits multiple VSWR minima below 2 across the operating range. Each minimum corresponds to a distinct resonant band identified in the S_{11} analysis. Impedance matching remains within acceptable limits across these bands, supporting consistent multiband operation. The VSWR trends are consistent with the reflection coefficient results and further indicate that the Rogers substrate supports more stable multiband behaviour under identical geometric conditions.

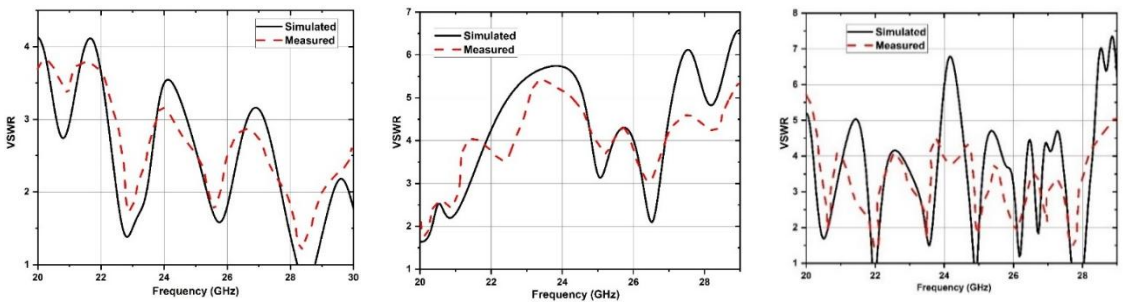

Fig. 5. VSWR Plots of hexagonal ring for Duroid, FR4 & Rogers

International Journal of Emerging Research in Engineering, Science, and Management
Vol. 5 | Issue 1 | pp. 32-41 | Jan-Mar 2026.
www.ijeresm.com | eISSN – 2583-4894
Received: 22 Nov 2025 | Revised: 16 Feb 2026 | Accepted: 23 Feb 2026 | Published: 01 Mar 2026

3.3. Gain Characteristics

The simulated realised gain responses are presented in Fig. 6. Duroid consistently shows the highest and most stable gain among the three substrates. The radiation patterns are smooth with minimal distortion. Cross-polarisation levels are comparatively lower. This indicates efficient radiation of the accepted power, making Duroid suitable for high-gain applications. The FR4 configuration exhibits noticeably lower gain values. The radiation patterns show irregularities and relatively higher cross-polarisation levels. Performance degradation is more evident at higher frequencies. This behaviour is attributed to increased dielectric losses, which reduce radiation efficiency at millimetre-wave frequencies. The Rogers substrate provides gain values slightly lower than Duroid but remains consistent across multiple resonant bands. Each resonant band exhibits stable and usable gain characteristics. The radiation patterns remain reasonably well controlled. This suggests that Rogers offers a balanced trade-off between peak gain and multiband capability. Duroid provides the highest gain, FR4 exhibits reduced radiation performance, and Rogers maintains consistent gain across multiple operating bands.

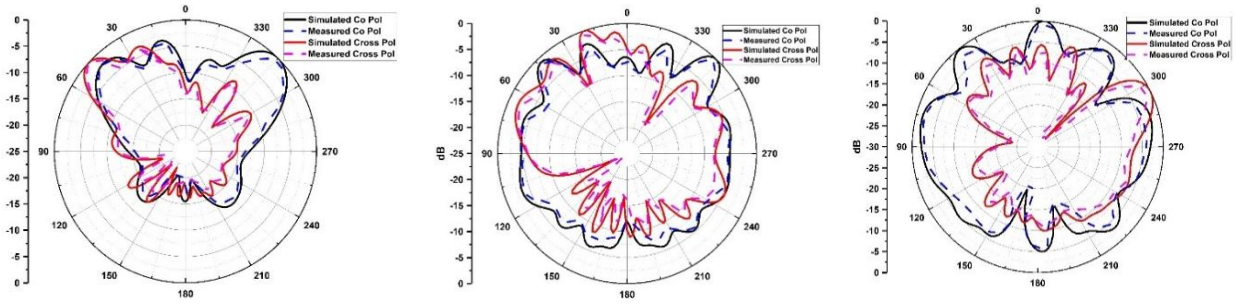

Fig. 6. Gain Plots of hexagonal ring for Duroid, FR4 & Rogers

When the S_{11}, VSWR, and gain responses are analysed together, it can be observed that each substrate supports different performance characteristics. Duroid achieves strong impedance matching and higher gain but supports fewer resonant modes. Although cost-effective, FR4 exhibits higher dielectric losses and reduced radiation performance at mmWave frequencies. Rogers, while slightly lower in peak gain compared to Duroid, supports stable multiband operation with acceptable radiation performance. From an application perspective, Rogers may be considered for compact multiband mmWave devices, Duroid for high-gain communication or radar systems, and FR4 for lower-frequency or cost-sensitive prototype implementations.

3.4. Surface Current Distribution

Fig. 7 illustrates the surface current distribution at the dominant resonant frequencies for each substrate. The surface current distribution for the Duroid-based configuration exhibits strong current concentration along the microstrip feed line and the outer edges of the hexagonal ring, indicating efficient impedance coupling and dominant edge-mode excitation. The maximum current density reaches 92.77 A/m, with smooth and relatively uniform current flow across the radiating element. The absence of significant localised current damping regions suggests minimal dielectric loss, consistent with Duroid's low loss tangent ($\tan\delta \approx 0.0009$). The defected ground structure (DGS) perturbs the return current path beneath the patch, introducing additional reactive loading that enhances resonance formation and supports multiband behaviour. The well-confined current distribution contributes to improved radiation efficiency and realised gain at mmWave frequencies.

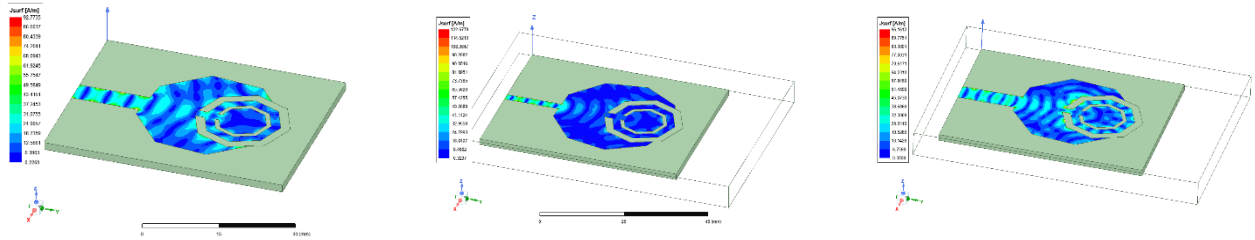

Fig. 7. Surface Current Distribution for Duroid, FR4 & Rogers

The FR4-based configuration exhibits pronounced current concentration along the feed line and hexagonal ring edges, indicating proper excitation of the radiating element. Although the peak surface current density reaches approximately 122.68 A/m, the distribution is more localised and less uniform compared to the low-loss substrates. This behaviour suggests stronger reactive energy storage near the excitation region, while dielectric losses ($\tan\delta \approx 0.02$) attenuate the propagation of surface waves across the patch.

International Journal of Emerging Research in Engineering, Science, and Management
Vol. 5 | Issue 1 | pp. 32-41 | Jan-Mar 2026.
www.ijeresm.com | eISSN – 2583-4894
Received: 22 Nov 2025 | Revised: 16 Feb 2026 | Accepted: 23 Feb 2026 | Published: 01 Mar 2026

The DGS modifies the ground-current path and assists with resonance tuning; however, the higher dielectric loss reduces the effective radiation efficiency despite strong localised excitation. Consequently, while FR4 supports resonance formation, increased dielectric dissipation limits the preservation of electromagnetic energy and the realized gain at mmWave frequencies. The Rogers-based configuration demonstrates strong and smoothly distributed surface current along the feed line and the hexagonal ring edges, indicating efficient impedance coupling and edge-mode excitation. The maximum surface current density of approximately 96.16 A/m reflects effective energy confinement with moderate dielectric attenuation. Compared to FR4, the current distribution is more uniform and less localised, suggesting improved electromagnetic energy propagation across the radiator. The DGS introduces a controlled perturbation into the return-current path, facilitating resonance tuning and stable multiband operation. The balanced dielectric properties of Rogers support improved radiation efficiency relative to FR4 while maintaining modal stability and consistent realised gain.

3.5. Radiation Efficiency and Total Efficiency

The radiation efficiency and total efficiency characteristics of the Duroid-based hexagonal DGS antenna are illustrated in Fig. 8. The red curve represents radiation efficiency, while the green curve denotes total efficiency over the 22–28 GHz operating band. The radiation efficiency remains consistently high across the operating band, exceeding 95% at the resonant frequencies. This behaviour indicates minimal dielectric dissipation in the low-loss Duroid substrate and effective radiation of the accepted power. The total efficiency, which accounts for both radiation and impedance-mismatch losses, ranges from approximately 60% to 85% across the band. Efficiency peaks near the resonant frequencies at 23 GHz and 26–28 GHz, corresponding to improved impedance matching. The reduction in total efficiency at intermediate frequencies (around 24 GHz and 26.8–27 GHz) is primarily associated with impedance mismatch rather than dielectric loss, as indicated by the consistently high radiation efficiency. The separation between radiation efficiency and total efficiency curves suggests that performance variation is mainly influenced by reflection losses rather than material dissipation. The Duroid substrate exhibits high radiation efficiency and stable resonance behaviour within the intended mmWave band.

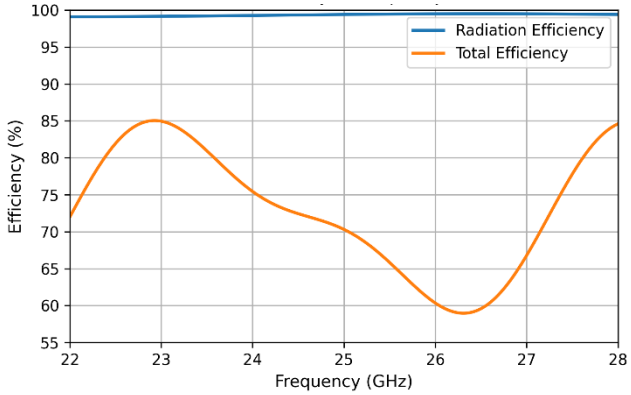

Fig. 8. Radiation Efficiency and Total Efficiency vs Frequency Plot

3.6. Key Contributions and Technical Insights

The results presented in this study provide several technical insights into substrate-controlled behaviour of DGS-integrated millimetre-wave patch antennas. By maintaining identical antenna geometry across Duroid, Rogers, and FR4 substrates, the investigation isolates the direct influence of dielectric constant and loss tangent on resonance formation, impedance behaviour, radiation efficiency, and realised gain. This controlled configuration enables clear attribution of performance variations to substrate properties rather than structural modification.

The analysis demonstrates that low-loss substrates support sharper resonances and higher radiation efficiency, whereas moderate-permittivity substrates enable stable multiband excitation under fixed geometric conditions. In contrast, higher-loss materials exhibit reduced resonance depth and gain degradation at mmWave frequencies due to dielectric attenuation. The incorporation of a defected ground structure (DGS) introduces controlled reactive perturbation in the ground plane, reducing the effective quality factor and improving impedance bandwidth without altering overall antenna geometry. The equivalent LC modelling further supports the resonance behaviour observed in full-wave simulations. The study establishes a substrate-focused evaluation approach for compact 5G FR2 antenna design, highlighting the role of dielectric properties in balancing impedance stability, multiband response, and radiation performance.

International Journal of Emerging Research in Engineering, Science, and Management
Vol. 5 | Issue 1 | pp. 32-41 | Jan-Mar 2026.
www.ijeresm.com | eISSN – 2583-4894
Received: 22 Nov 2025 | Revised: 16 Feb 2026 | Accepted: 23 Feb 2026 | Published: 01 Mar 2026

4 CONCLUSION

A substrate-dependent performance investigation of a DGS-integrated hexagonal microstrip patch antenna operating in the 22–28 GHz band has been presented. By maintaining identical geometry across Duroid, Rogers, and FR4 substrates, the study isolates the impact of dielectric constant and loss tangent on resonance formation, impedance behaviour, radiation efficiency, and realised gain. The comparative analysis indicates that low-loss substrates enhance the preservation of electromagnetic energy at millimetre-wave frequencies. The Duroid-based configuration exhibits deep impedance minima (below −32 dB), high realised gain (8–8.5 dBi), and consistently high radiation efficiency, suggesting minimal dielectric dissipation and stable modal excitation. The Rogers substrate demonstrates controlled multiband response with acceptable impedance matching and moderate gain, representing a practical balance between performance and manufacturability. In contrast, the FR4 substrate exhibits increased dielectric attenuation, resulting in reduced resonance depth, lower gain, and decreased radiation efficiency, thereby limiting its effectiveness at mmWave frequencies. The results show that substrate permittivity and loss tangent influence not only impedance characteristics but also resonance sharpness, quality factor, and modal stability in DGS-based multiband antennas. The presented substrate-controlled evaluation approach may assist designers in selecting appropriate dielectric materials for compact 5G FR2 antenna implementations where efficiency, bandwidth stability, and gain performance are important considerations.

FUNDING INFORMATION

This research received no specific grant from any funding agency in the public, commercial, or not-for-profit sectors.

ETHICS STATEMENT

This study did not involve human or animal subjects and, therefore, did not require ethical approval.

STATEMENT OF CONFLICT OF INTERESTS

The authors declare no conflicts of interest related to this study.

REFERENCES

[1] D. M. Pozar, "Microstrip antennas," in *Proceedings of the IEEE*, vol. 80, no. 1, pp. 79-91, Jan. 1992, doi: 10.1109/5.119568.

[2] S. Sadasivam, V. T. Bai, R. Yuvaraj, P. S. Rahul, and M. R. Thomas, "Comparison of FR4 and Roger substrates in multiband two-slot rectangular patch antenna for 5G applications," *Materials Today Proceedings*, vol. 55, pp. 452–454, Jan. 2022, doi: 10.1016/j.matpr.2021.12.600.

[3] G. S. Deepthy and M. Nesasudha, "Analysis of substrate materials in microstrip antenna for biomedical applications," *Materials Today Proceedings*, Jan. 2023, doi: 10.1016/j.matpr.2023.01.130.

[4] M. Sharma, B. R. Perli, L. Matta, T. Addepalli, K. Sharma, and F. N. Sibai, "Flexible four-port MIMO antenna for 5G NR-FR2 tri-band mmWave application with SAR analysis," *Scientific Reports*, vol. 14, no. 1, p. 29100, Nov. 2024, doi: 10.1038/s41598-024-79859-1.

[5] N. A. Alqwaifly, W. A. Awan, N. Alsaab, F. N. Alsunaydih, and K. Alhassoon, "Array inspired wideband and high gain antenna with enhanced pattern diversity for 5G mm wave networks," *Scientific Reports*, vol. 15, no. 1, p. 27383, Jul. 2025, doi: 10.1038/s41598-025-12868-w.

[6] M. K. Woo *et al*., "Evaluation of a 16-Channel Transceiver Loop + Dipole Antenna Array for Human Head Imaging at 10.5 Tesla," in *IEEE Access*, vol. 8, pp. 203555-203563, 2020, doi: 10.1109/ACCESS.2020.3036598.

[7] E. C. Gözek, F. Tokan, and M. Karaaslan, "Frequency Reconfigurable Lıbra Shape Antenna for mmW 5 g Communıcatıons," *Journal of Infrared Millimeter and Terahertz Waves*, vol. 46, no. 7, Jul. 2025, doi: 10.1007/s10762-025-01064-6.

[8] C. K. Ali and M. H. Arif, "Dual-band Millimeter-Wave Microstrip Patch Array Antenna for 5G Smartphones," *2019 International Conference on Advanced Science and Engineering (ICOASE)*, Zakho - Duhok, Iraq, 2019, pp. 181-185, doi: 10.1109/ICOASE.2019.8723719.

[9] H. El-Hakim and H. A. Mohamed, "Synthesis of a multiband microstrip patch antenna for 5G wireless communications," *Journal of Infrared Millimeter and Terahertz Waves*, vol. 44, no. 9–10, pp. 752–768, Aug. 2023, doi: 10.1007/s10762-023-00937-y.

[10] A. S. Al-Hiti, A. K. Ahmed, S. H. Mhmood, and B. I. Hamdallah, "Broadband and multiband millimeter wave microstrip patch antenna for 5G and 6G applications," *Journal of Umm Al-Qura University for Engineering and Architecture*, vol. 16, no. 3, pp. 720–731, Jul. 2025, doi: 10.1007/s43995-025-00161-w.

[11] M. El-Amine Mahlia, S. Mekaoui and M. L. Tounsi, "Enhancing 5G Millimeter-Wave Multiband Capabilities with Optimized Microstrip 4x4 Array Antenna," *2024 IEEE International Symposium on Phased Array Systems and Technology (ARRAY)*, Boston, MA, USA, 2024, pp. 1-8, doi: 10.1109/ARRAY58370.2024.10880365.

International Journal of Emerging Research in Engineering, Science, and Management
Vol. 5 | Issue 1 | pp. 32-41 | Jan-Mar 2026.
www.ijeresm.com | eISSN – 2583-4894
Received: 22 Nov 2025 | Revised: 16 Feb 2026 | Accepted: 23 Feb 2026 | Published: 01 Mar 2026

[12] B. Gong, Z. Fang, K. Lu, N. Yang and P. Pan, "Broadband Dual-Layer Patch Antenna for Millimeter-Wave Antenna-in-Package Applications," *2024 Cross Strait Radio Science and Wireless Technology Conference (CSRSWTC)*, Macao, China, 2024, pp. 1-3, doi: 10.1109/CSRSWTC64338.2024.10811515.

[13] A. Modi, V. Sharma and A. Rawat, "Compact Design of Multiband Antenna for IRNSS, Satellite, 4G and 5G Applications," *2021 5th International Conference on Computing Methodologies and Communication (ICCMC)*, Erode, India, 2021, pp. 6-9, doi: 10.1109/ICCMC51019.2021.9418265.

[14] R. Shrivastava and A. Khare, "Design of Hexagonal Wideband Microstrip Patch Antenna for MIMO Wireless Applications," *2023 14th International Conference on Computing Communication and Networking Technologies (ICCCNT)*, Delhi, India, 2023, pp. 1-5, doi: 10.1109/ICCCNT56998.2023.10308371.

[15] M. S. Yahya *et al.*, "LoRa Microstrip Patch Antenna: A comprehensive review," *Alexandria Engineering Journal*, vol. 103, pp. 197–221, Jun. 2024, doi: 10.1016/j.aej.2024.06.017.

[16] R. H. Elabd, A. J. A. Al-Gburi, and A. A. Megahed, "Compact circular MIMO antenna with defected ground structure (DGS) for improved isolation in 5G sub-6GHz mobile systems," *Results in Engineering*, vol. 27, p. 105737, Jun. 2025, doi: 10.1016/j.rineng.2025.105737.